

1 **Pore-scale fluid dynamics resolved in pressure**
2 **fluctuations at the Darcy scale**

3 **Catherine Spurin¹, Gareth G. Roberts², Conor P. B. O'Malley², Takeshi**
4 **Kurotori^{1,3}, Samuel Krevor², Martin J. Blunt², and Hamdi Tchelepi¹**

5 ¹Department of Energy Science & Engineering, Stanford University

6 ²Department of Earth Science & Engineering, Imperial College London

7 ³Department of Chemical Engineering & Engineering, Imperial College London

Corresponding author: Catherine Spurin, cspurin@stanford.edu

Abstract

Complex flow dynamics have been observed, at the pore-scale, during multiphase through porous rocks. These dynamics are not captured in large scale models exploring the migration and trapping of subsurface fluids e.g., CO₂ or hydrogen. Due to limitations in imaging capabilities, these dynamics cannot be observed directly at the larger, Darcy scale. Instead, by using pressure data from pore-scale (mm-scale) and core-scale (cm-scale) experiments, we show that fluctuations in pressure measured at the core-scale reflect specific fluid displacement events taking place at the pore-scale. The spectral characteristics of the pressure data depends on the flow dynamics, size of the rock sample, and heterogeneity of pore space. While high resolution imaging of large samples would be useful in assessing flow dynamics across many of the scales of interest, such an approach is currently infeasible. We suggest an alternative, pragmatic, approach examining pressure data in the time-frequency domain using wavelet transformation.

Plain Language Summary

Complex fluid dynamics have been observed in small pores within rocks. These dynamics have not been accounted for in larger scale modelling efforts of CO₂ or hydrogen. Limitations in imaging prevent the direct observation of these dynamic at larger scales, creating uncertainty in how these dynamics manifest at larger scales. But by analyzing the pressure data, and fluctuations in pressure measurements, we can infer the small-scale dynamics without imaging. We apply our findings to larger samples and discover that the fluctuations are dependent on the type of flow dynamics occurring, sample size, and the composition of the sample. We present a practical approach for assessing the dynamics at the larger scale, where direct imaging is currently infeasible, by exploring the pressure data using a technique called continuous wavelet transformation.

1 Introduction

Fluid flow in the subsurface is a complex process, controlled by the interaction of multiple fluids with one another, and a heterogeneous pore space. It is central to the safe storage of CO₂ in the subsurface (Rubin & De Coninck, 2005; Bachu & Adams, 2003; Benson et al., 2012), and the storage and retrieval of hydrogen underground (Boon & Hajibeygi, 2022; Thiyagarajan et al., 2022), as examples. Depending on the flow rate, fluid viscosity, wettability of the fluids, and connectivity of the pore space, different flow mechanisms will prevail (Blunt, 2017; Lenormand et al., 1983; Avraam & Payatakes, 1995; Spurin et al., 2019a, 2019b; Rucker et al., 2015; Zou et al., 2018; Zhao et al., 2016). These processes span many orders of magnitudes for both timescales and length scales, from sub-second to hours (Berg et al., 2013; Schlüter et al., 2017; McClure et al., 2020), and sub-pore to multi-pore (Berg et al., 2013; Moebius & Or, 2014; Spurin et al., 2020). Fluid flow is also heavily controlled by the heterogeneity of the rock, which in itself ranges from nanometers to kilometers (Ringrose & Bentley, 2016; Jackson et al., 2018).

This complexity makes modelling the flow and trapping of fluids in the subsurface challenging, with uncertainty in which flow processes are important to characterise at different spatial scales. For example, at the scale of a reservoir, many attempts to predict CO₂ plume migration in the subsurface resulted with the CO₂ arriving earlier and spreading out further than expected (Dance et al., 2019; Hosseini et al., 2013; Daley et al., 2011; Ringrose et al., 2013). These analyses focused on characterising heterogeneity in continuum-scale properties, like capillary pressure and relative permeability (Jackson & Krevor, 2020). However, observations made at the pore-scale show dynamics that are not incorporated within the framework of continuum-scale flow properties, such as intermittent pathway flow and ganglion dynamics (Spurin et al., 2019a, 2019b; Rucker et al., 2015; Gao et al., 2020; Avraam & Payatakes, 1995). Traditional continuum-scale models relate flow rate linearly to an average pressure gradient across the system. They do

not account for any fluctuations in pressure, or a non-linear relationship between flow rate and pressure gradient, both of which have been observed experimentally, and attributed to non-linear flow dynamics (Blunt, 2017; Muskat, 1938; Zhang et al., 2021). These dynamics may play a role in large-scale flow properties, and will influence plume migration (Spurin et al., 2020; Juanes et al., 2010; Zhang et al., 2021).

Micro-computed tomography (Micro-CT) experiments provide pore-scale observations of fluid-fluid interfaces *in situ* at resolutions of a few microns. However, experimental limitations including temporal resolution, expense, and management of vast quantities of data produced, mean it is currently infeasible to observe fluid-fluid interfaces at the centimetre to metre scale (the core-scale). Instead, medical CT scanners are used to measure saturation distributions (Akin & Kavscek, 2003; Pini & Madonna, 2016; Krevor et al., 2012). If observations of flow from pore-scale experiments are representative of flow at larger scales they can, in principle, be used to understand results from core-scale experiments. However, it is unclear if information about flow dynamics is being lost due to the limited spatial and temporal scales of the pore-scale experiments, or if pore-scale dynamics differ when sample size is increased. For example, viscous and gravity forces may become more important at larger scales, even in capillary-dominated regimes.

Pore-scale and core-scale experiments have two overlapping quantities that are measured: saturation and pressure. Saturation is important, as it can indicate the amount of trapping, but without a measure of connectivity, it gives no indication of the underlying dynamics. However, pressure fluctuations have been related to pore-scale dynamics and energy dissipation in the pore space through the creation and destruction of interfaces (Spurin et al., 2022; Rücker et al., 2021). In this work, we explore how pressure fluctuations measured during core-scale experiments can be used to provide insight into underlying flow dynamics by using continuous wavelet transforms to map the spectral power of pressure data. We identify sources of spectral power as a function of time and frequency. The merits of using pressure data to obtain information about multiphase flow in porous media, including possible scaling relationships, are assessed.

2 Methods

2.1 Experimental Procedure

The experiments in this work were conducted at two different scales: the pore-scale and the core-scale. For the pore-scale investigation, the sample was a carbonate rock, 5 mm in diameter and 20 mm long. These experiments were conducted at a synchrotron facility, so fluid interfaces could be resolved in real time (Spurin et al., 2020). There are two experiments in the pore-scale investigation, which both explored the transition to steady-state dynamics. One observes intermittent pathway flow through the co-injection of gas and water, while the other observes connected pathway flow through the co-injection of oil and water (Spurin et al., 2021, 2020). The capillary number, defined as $Ca = q/\sigma\lambda$ where q is the flow rate, σ is the interfacial tension and λ is the mobility of the fluids was 1.6×10^{-7} for the gas/water experiments and 2.2×10^{-6} for the oil/water experiments. See Spurin et al. (2020) for a full experimental description.

For the core-scale investigation, the sample was a carbonate rock, 5 cm in diameter and 12 cm long. The experiments were conducted in a medical CT scanner, so the fluid interfaces themselves cannot be resolved, but the saturation across many pores is measured (see Figure 1 for the difference in imaging resolution at the different scales). Three experiments were performed to explore the transition to steady-state dynamics; two explore the co-injection of gas and water. The same sample was used for both these experiments, but the sample orientation was reversed between experiments, to explore the role of heterogeneity of the pore space on flow dynamics. For the third experiment oil and water were co-injected. Sample orientation was not reversed in this experiment

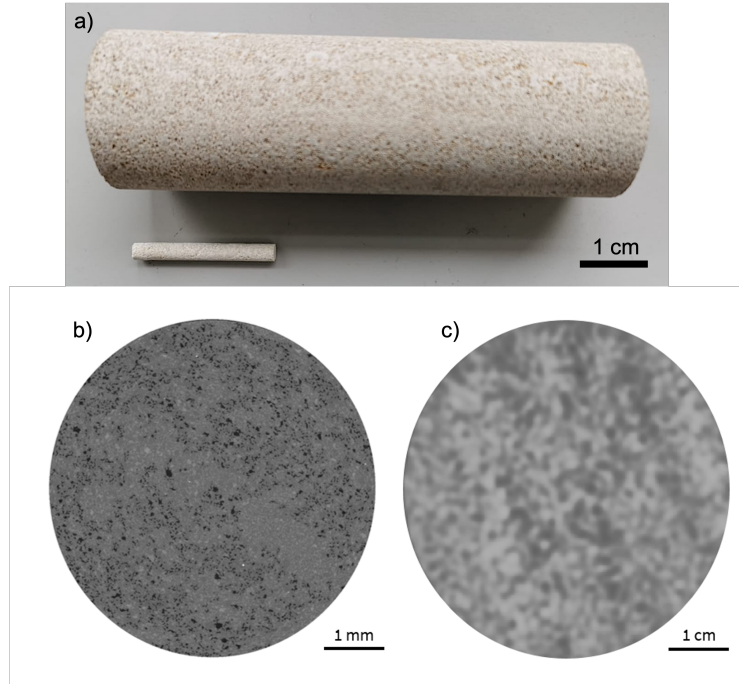


Figure 1. (a) The core-scale (large) sample shown alongside the pore-scale sample to highlight the difference in scale. (b) A CT slice through the pore-scale sample, where fluid interfaces are resolvable. (c) A CT slice through the core-scale sample, where fluid interfaces are not resolvable but grayscale values are proportion to saturation.

108 as oil is difficult to remove from a sample, which would have influenced the observations.
 109 The capillary number was 2.0×10^{-8} for the gas/water experiments and 5.4×10^{-7} for
 110 the oil/water experiment. With similar capillary numbers, we aimed to observe the same
 111 manifestation of the pore-scale dynamics in the pressure data as the pore-scale exper-
 112 iments. The full experimental procedure is provided in the Supplementary Material.

113 An example of the images taken during an experiment at each scale is shown in Fig-
 114 ure 1. It highlights the impact of the different imaging resolutions for the experiments,
 115 and shows how connectivity of the fluid phases cannot be calculated from traditional med-
 116 ical CT imaging. Thus, due to these imaging constraints, the only parameters that are
 117 constant across the experimental scales are saturation and pressure. The pressure drop
 118 across the the sample with time is the parameter of interest in this work, and was recorded
 119 for all experiments using a differential pressure transducer connected to the inlet line for
 120 the water, and the outlet line for both phases.

121 2.2 Spectral Analysis Using Wavelet Transformation

122 The spectral content of the pressure data was investigated by transforming it into
 123 the frequency-time domain using a continuous wavelet transformation (CWT). This dif-
 124 fers from previous work using Fourier transformation of pressure data that revealed a
 125 cascade of timescales for steady-state multiphase flow, with lower frequency events hav-
 126 ing larger amplitudes (Spurin et al., 2022). While insightful, Fourier transforms have some
 127 limitations that make further analysis difficult. These include significant power spectral
 128 leakage, noisy calculated power spectra, and the fact that stationary functions are un-
 129 likely to reflect changes in pressure as a result of flow, especially during transient flow,

130 when average pressure is a function of time. Mapping spectral power as a function of fre-
 131 quency and time might provide additional insight into the dynamics of the system

132 We use a transform that convolves a uniformly-sampled pressure data time series,
 133 p_t , with a mother wavelet, ψ . Pressure time series, with constant sampling intervals of
 134 either $\delta_t = 1.29$ seconds (pore-scale experiments; Figure 2) or 9.3 seconds (core-scale
 135 experiments; Figures 3 & 4), were mirrored 7 times before being transformed to ame-
 136 liorate edge effects (Roberts et al., 2019). The Derivative-of-Gaussian (DOG) wavelet,
 137 with derivative $m = 6$, was used as the mother wavelet in this study. It was scaled and
 138 translated along the time series by t' to reveal variations in amplitude as a function of
 139 scale, s , and time, t . Thus, the wavelet transform, $W_t(s)$, has the form:

$$W_t(s) = \sum_{t'=0}^{N-1} p_t \psi^* \left[\frac{(t' - t)\delta t}{s} \right] \quad (1)$$

140 where ψ^* denotes the complex conjugate of the mother wavelet. N is the number
 141 of discrete measurements of pressure. In this study, $N = 385$ for the gas/water core-
 142 scale experiments (total sampling duration ≈ 1 hour), for the oil/water core experiment
 143 $N = 577$ (≈ 1.5 hours). For the pore-scale experiments $N = 24,991$ (≈ 9 hours) and
 144 14,081 (≈ 4 hours) for gas/water and oil/water experiments, respectively. The code was
 145 adapted from O'Malley and Roberts (2022), and based on the methods summarized by
 146 Torrence and Compo (1998). The input signals can be recovered with errors less than
 147 2.5% via the inverse transform, highlighting the fidelity of the transformations (see Sup-
 148 plementary Material).

149 The wavelet transform can be converted into power, ϕ , such that $\phi(t, s) = |W_t(s)|^2$.
 150 The time-averaged power spectrum is thus:

$$\phi(s) = \frac{1}{N} \sum_{t=0}^{N-1} |W_t(s)|^2. \quad (2)$$

151 Following (Liu et al., 2007), power is rectified by scale, and scales are converted into
 152 equivalent Fourier frequencies. The rectified time-averaged power spectra, $\phi_r = \phi(s)s^{-1}$,
 153 are consistent with results obtained from Fourier transformation of the time series.

154 Relationships between power spectral amplitudes and frequencies, f , provide in-
 155 sight into the scaling regimes and dynamics of many physical systems (Moura et al., 2017;
 156 Spurin et al., 2022; Rudnick & Davis, 2003; Fernandes et al., 2022; van der Schaaf et al.,
 157 2002). Many geophysical time series are characterised by:

$$\phi_r \propto f^\alpha. \quad (3)$$

158 Determining the value(s) of α from the power spectra of time series can be a con-
 159 venient way to identify scaling regime(s). For example, $\alpha = -2$ indicates that a time
 160 series can be characterized as red noise. If pressure time series are characterized by red
 161 noise, it implies that the amplitudes of the pressure perturbations are proportional to
 162 their duration. White noise, $\alpha = 0$, indicates that the amplitudes of pressure pertur-
 163 bations are roughly the same across all frequencies. A variety of other noise distributions
 164 and changing patterns of spectral content can be straightforwardly identified by plot-
 165 ting power as a function of frequency in log-log space. For example, black, pink, and blue
 166 noise have spectral slopes, α , of -3 , -1 and 1 , respectively.

3 Results and Discussion

3.1 Sources of Spectral Power

There are many different potential sources for the spectral power in pressure time series during multiphase flow. The main ones identified here are (1) flow mechanisms (such as intermittent pathway flow or connected pathway flow), (2) heterogeneity of the pore space, and (3) the ratio of capillary to viscous forces.

In this research we focus on the flow mechanisms, and their representation in pressure signals in pore-scale experiments. This approach allows us to link spectral power to different flow regimes. We explore if the spectral scalings obtained can be applied to core-scale results to assess whether flow regimes can be deduced without pore-scale imaging. With the larger samples, we explore the role of heterogeneity on fluid flow by repeating the experiment with the sample orientation reversed, so that the direction of flow relative to the heterogeneity is reversed. Note that the degree and orientation of heterogeneity is linked to the flow mechanisms (Spurin et al., 2019a), so it is non-trivial to isolate them. With larger cores, viscous forces may also play a more important role.

3.2 Pore-Scale Results

The results for the pore-scale experiments are shown in Figure 2, with panels a-d showing the results for the gas/water experiment and panels e-h showing the results for the oil/water experiment. Panels a and e in Figure 2 show the pressure drop across the sample recorded during an experiment for gas/water and oil/water, respectively. The shaded green strips correspond to the time intervals for the time-averaged power spectra shown in panels d and h, with a later time denoted by a darker shade. Note these panels indicate ~ 1 hr intervals for the gas/water experiment, and ~ 30 min intervals for the oil/water experiment because steady-state was reached quicker during the oil/water experiment. Figure 2b and f show power spectra of pressure data with time for gas/water and oil/water, respectively. Here, the dashed lines correspond to the shaded green strips in panels a and e. Figure 2c-d and g-h show time-averaged power against frequency for gas/water and oil/water, respectively. This is shown for the full recording window, and the 1st and 2nd half of the pressure time series in Figure 2c and g, which can be compared to the evolution of the power spectra for shorter intervals in Figure 2d and h.

With the pore-scale experiments, we can relate power spectra to different flow regimes observed during the experiments. For both experiments, the sample is initially saturated with water. First, the non-wetting phase (the gas or oil) percolates the sample, resulting in purely drainage events (gas or oil displacing the water). At approximately 20,000 s for the gas/water experiment (Figure 2a) and 3,000 s for the oil/water experiment (Figure 2e) the pressure plateaus, marking the transition to steady-state flow. For the gas/water experiment this leads to intermittent pathway flow, where gas flow pathways repeatedly connect and disconnect (Spurin et al., 2020). For the oil/water experiment no further displacement events occur during steady-state flow; the fluids flow in their own separate pathways that are connected across the pore space (Spurin et al., 2020).

3.2.1 Intermittent Pathway vs Connected Pathway Flow

For the gas/water experiment fluid rearrangement events were larger and occurred even during steady-state flow, while the oil/water experiment had little to no fluid rearrangement once oil had percolated the sample (Spurin et al., 2020, 2022). The different flow regimes are evident in the pressure in Figure 2a and e. First, in the oil/water experiment the pressure overshoots the stabilisation pressure (at around 3,000 s in Figure 2e), but then relaxes to approximately 65 kPa for the rest of the experiment. In the gas/water experiment, the pressure builds more gradually and then plateaus at approximately 20,000 s in Figure 2a. There are significantly more fluctuations during the gas/water

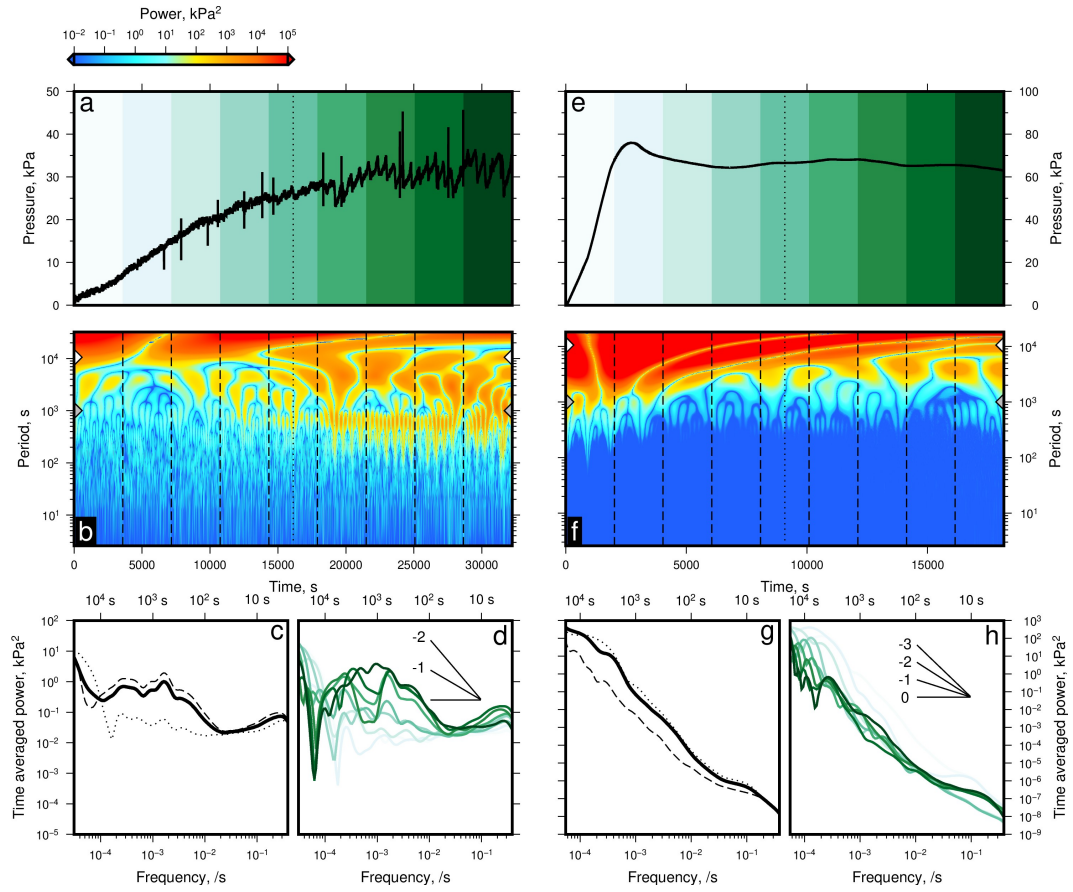


Figure 2. Spectral analysis of pressure time series from pore-scale experiments. (a) Black curve = pressure from gas/water experiment. Green strips and dotted line = time intervals indicated in panels b-d. (b) Power spectrum calculated by transforming black curve in panel a. Dashed and dotted lines correspond to time intervals indicated in panel a. Grey/white arrow heads indicate limit on low pass filters (10^3 and 10^4 s) discussed in body text. (c) Thick black curve = time-averaged, rectified, power spectrum for entire series. Dotted and dashed curves = time-averaged power for 1st and 2nd half of the time series, respectively (separated by dotted line in panels a and b). (d) Time-averaged power spectra for intervals indicated by green strips in panel a. Note graticule indicating red (-2), pink (-1) and white (0 ; flat) spectral slopes. (e-h) Results for the oil/water experiment.

216 experiment, even if the mean pressure remains constant, due to intermittent gas path-
 217 ways periodically connecting and disconnecting.

218 Variations in the pressure time series are highlighted by the power spectra, pro-
 219 duced by the continuous wavelet transformation, shown in Figure 2b and f. Several re-
 220 sults are evident in the wavelet power spectra, which were not immediately obvious from
 221 inspection of the pressure time series alone. First, pressure at the longer periods/lower
 222 frequencies increases in power as the system transitions to steady-state for the exper-
 223 iment with intermittency (shown by the increase in power at periods of approximately
 224 10^3 s in Figure 2b). This observation corresponds to the approximately 10 minute cy-
 225 cles observed in the pressure data in Figure 2a). These cycles were linked to disconnec-
 226 tion and re-connection events in a key location, controlling flow across the sample (Spurin
 227 et al., 2020).

228 Secondly, pressure at shorter periods/higher frequencies contributes less to total
 229 power than the longer period fluctuations. Consider that inverse wavelet transforms pro-
 230 duced including periods $> 10^3$ s have a mean error, which we define here as

$$\frac{1}{N\bar{p}_t} \sum_{t=1}^N \left[(p_t - p_{tf})^2 \right]^{1/2} \times 100(\%), \quad (4)$$

231 where p_{tf} are pressures in the filtered series and \bar{p}_t is mean pressure of the unfil-
 232 tered series, of only 3% for the gas/water experiment (Figure 2b: grey arrow heads). The
 233 mean error is even less (2%) for the oil/water experiment (Figure 2f: grey arrow heads).
 234 Inverse transforms with only periods $> 10^4$ s included yield a mean error of 5% for the
 235 gas/water experiment, and 8% for the oil/water experiment (white arrow heads in Fig-
 236 ure 2b and f, respectively). Shorter period variations in pressure ($< 10^3$ s), whilst still
 237 providing relatively little overall power, account for a greater proportion of the total power
 238 in the gas/water experiments compared to the oil/water experiment. In contrast, longer
 239 periods ($> 10^4$ s) contribute a relatively larger proportion of the total power for the oil/water
 240 experiment. In summary, pressure fluctuations at short periods play a greater role in larger
 241 scale flow properties in the gas/water experiment compared to in the oil/water exper-
 242 iment. This observation is indicative of the role that the pore-scale intermittency has
 243 in enabling flow at relatively little energy cost (Spurin et al., 2021).

244 Finally, time-averaged power spectra (Figure 2c-d and g-h) show that, for the gas/water
 245 experiment, different spectral slopes exist as the system evolves to steady-state condi-
 246 tions, transitioning from a slope of -1 (pink noise) to -2 (red noise) in Figure 2d, whilst
 247 a roughly constant spectral slope exists at all times and across all timescales during the
 248 oil/water experiment. This observation highlights the complexity of intermittent path-
 249 way flow, with events occurring over a wide range of frequencies, length-scales, and be-
 250 ing non-local in nature (Spurin et al., 2020). At steady-state, intermittent pathway flow
 251 manifests as red noise (a spectral slope of -2) and connected pathway flow manifests as
 252 a spectral slope of -3 . A slope of -2 agrees with observations made using Fourier trans-
 253 formation on steady-state pressure data (Spurin et al., 2022). A slope of -3 is typical
 254 for pseudo-turbulent flows (Mercado et al., 2010; Roghair et al., 2011; Mendez-Diaz et
 255 al., 2013). These are flows that appear turbulent but are in fact the result of the com-
 256 plex interaction of fluids with the surrounding space (other fluids, and in this case, po-
 257 tentially the rock grains) instead of inertial forces (Mercado et al., 2010). Further research,
 258 including velocity measurements are required to determine if pseudo-turbulence is oc-
 259 ccurring in multi-phase flow through porous media.

260 **3.2.2 Possibility of Upscaling**

261 For the oil/water experiment, where both fluids flowed in continuously connected
 262 pathways (as assumed in the multiphase extension of Darcy’s law), a broadly constant

263 spectral slope of -3 exists for all frequencies during transient and steady-state flow (Fig-
 264 ure 2h). These observations imply that there is limited temporal evolution during con-
 265 nected pathway flow, creating less uncertainty in predictions made for periods outside
 266 the experimental observation window.

267 For the gas/water experiment, spectral slopes depend on frequency and time, which
 268 implies a change in dynamics at different periods and times (Figure 2d). Spectral slopes
 269 steepen at long ($> 10^4$ s) and short ($< 10^3$ s) periods as the system transitions to ‘steady-
 270 state’ flow. This highlights the presence of non-linear dynamics not included in the mul-
 271 tiphase extension of Darcy’s law. The presence of multiple spectral slopes makes sim-
 272 ple upscaling of predictions challenging. Thus, the success of upscaling efforts depends
 273 on how the dynamics present manifest in larger samples.

274 3.3 Core-Scale Results

275 The core-scale experiments follow the same procedure as the pore-scale experiments,
 276 with the same fluid pairings. This allows us to establish if the pore-scale observations
 277 can be upscaled to the core-scale experiments typically used for subsurface character-
 278 ization (Pini & Benson, 2013; Perrin et al., 2009; Ruprecht et al., 2014). Figure 3a-d shows
 279 the results for the gas/water experiment, e-h shows the results for the oil/water exper-
 280 iment and i-l shows the results for the gas/water experiment in which sample orienta-
 281 tion was reversed.

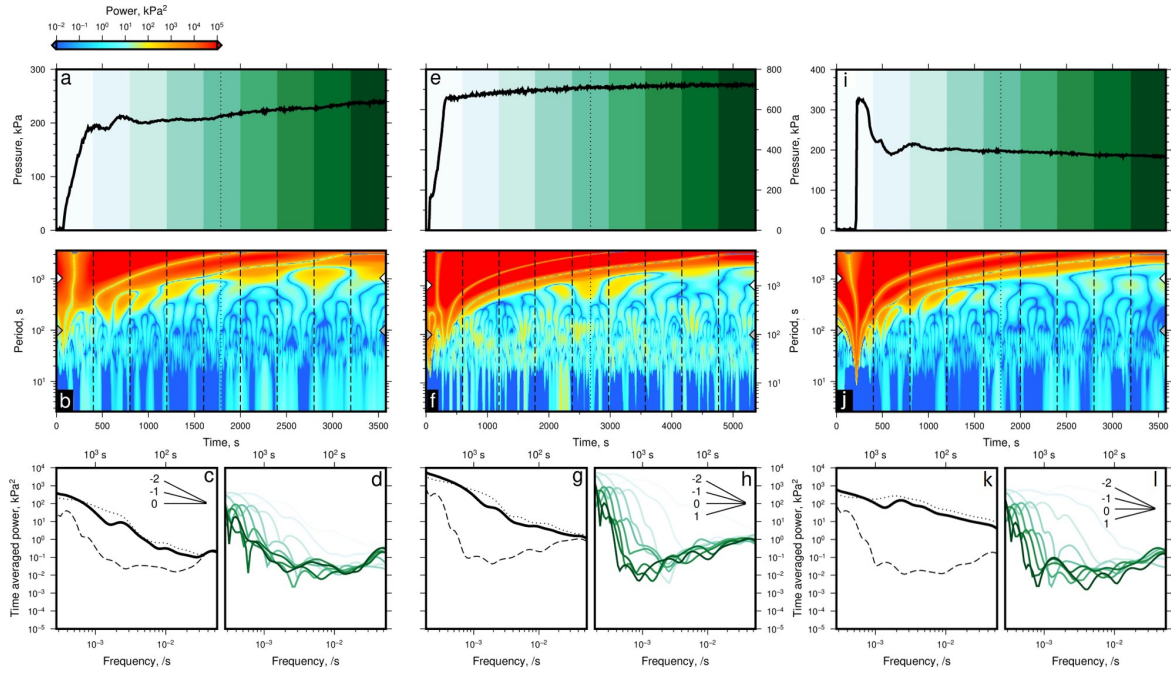


Figure 3. Spectral analysis of pressure time series from core-scale experiments. (a-d) Gas/water experiment initial sample orientation. (e-h) Oil/water experiment. (i-l) Gas/water experiment reversed sample orientation. Annotation is the same as Figure 2.

282 3.3.1 Gas/water vs Oil/water

283 The pressure response for the gas/water experiment and the oil/water experiment
 284 shown in Figure 3a and e appear similar in nature; in the first 500 s there is a steep in-
 285 crease in pressure as the gas or oil percolates the sample, then there is a gradual increase

286 in pressure with time, with pressure fluctuations of a similar magnitude (around 5 kPa).
 287 The spectral power provides additional insight into evolution of pressure, and reveals sub-
 288 tle differences between the experiments. First, power at longer periods ($> 10^3$ s) decreases
 289 with time, as shown by the reduction in red colours with increasing time in Figure 3b
 290 and f. Pressure at periods $> 10^3$ s contributes a similar proportion of power (mean er-
 291 ror $\sim 2\%$) in both the gas/water and oil/water experiments (white arrow heads in Fig-
 292 ure 3b and f). This implies that pressure at periods $> 10^3$ s contributes $\sim 98\%$ of to-
 293 tal power.

294 Power at frequencies of 3×10^{-2} to 2×10^{-3} Hz also decrease with time (Figure
 295 3d & h). Spectral slopes at these frequencies are observed to flatten (i.e. whiten). While
 296 longer periods contain less power at later experimental times, they continue to contribute
 297 significantly to the total power, shown by the spectral slope steepening as the system
 298 evolves in time. Pressure at shorter periods ($< 10^3$ s) contributes far less ($\sim 2\%$) to
 299 total power in both the oil/water and gas/water experiments.

300 When averaged over the entire experimental run time, as shown in Figure 3c and
 301 g, spectral power can be described by a single spectral slope of -2 i.e. red noise for both
 302 experiments. However, at the end of both experiments (the darkest green lines in Fig-
 303 ure 3d and h) the time-averaged power requires two spectral slopes, and differ for gas/water
 304 and oil/water, with a steeper spectral slope for frequencies $> 10^{-3}$ Hz for the latter.

305 **3.3.2 The Role of Heterogeneity**

306 The role of heterogeneity is evident in Figures 3a-d and i-l. In the experiment where
 307 the section of the sample with a lower porosity was closest to the inlet, there is an over-
 308 shoot in pressure prior to stabilisation (seen in Figure 3i) at approximately 200 s. Whereas,
 309 when flow direction is reversed, there is a gradual increase in pressure, and no marked
 310 overshoot, as shown in Figure 3a. Both experiments reach the same differential pressure
 311 of approximately 200 kPa within 15 minutes of injection.

312 For both experiments, pressure at lower frequencies decreases in power with time
 313 (shown in Figure 3d and l). Power is increasingly concentrated at lower frequencies dur-
 314 ing an experiment, regardless of the orientation of the sample. During steady-state flow,
 315 the spectral slope for higher frequencies ($< 10^{-3}$ Hz) resembles white noise i.e. the am-
 316 plitude is independent of frequency, while it is steeper for the lower frequencies. The spec-
 317 tral slope is -2 (red noise) when averaged over the whole time series. However, the evo-
 318 lution of the flow properties is dependent on the heterogeneity of the pore space and its
 319 orientation with respect to flow. This means that previous heterogeneity classifications,
 320 that rely on average porosity and permeability values for the whole core, miss the im-
 321 portance of the orientation of heterogeneity with respect to the flow direction (Li & Ben-
 322 son, 2015; Ni et al., 2019).

323 **3.4 Core-scale vs Pore-scale Results**

324 The magnitude of pressure fluctuations are similar for the core-scale and pore-scale
 325 experiments (they are on the order of 1–5 kPa). The total pressure drop is significantly
 326 higher for the core-scale experiments, meaning the pressure fluctuations are much smaller
 327 relative to the total pressure drop across the sample.

328 While the magnitude of pressure fluctuations are similar, spectral analysis reveals
 329 differences between the pore-scale and core-scale experiments. First, the single spectral
 330 slope observed in the pore-scale oil/water experiment is not observed in the core-scale
 331 oil/water experiment. While the spectral slope is approximately -3 for frequencies $<$
 332 10^{-3} Hz during steady-state flow at the core-scale, it flattens to 0 (white noise), for the
 333 higher frequencies/shorter periods (Figure 3h). This suggests that the shorter periods
 334 are less significant in the core-scale experiments during steady-state flow. Secondly, at

335 periods 10^2 to 10^4 s, power increases in the pore-scale gas/water experiment, while the
 336 shorter periods (down to ~ 10 s) remain approximately constant (Figure 2d). For the
 337 core-scale gas/water experiments, power decreases across almost all periods (down to \sim
 338 10 s), albeit at a slower rate. Thus the evolution of the time-averaged power spectra is
 339 dependent on scale. While similar spectral slopes are observable (between -1 and -3),
 340 these slopes are dependent on frequency and time. In all cases, the shorter timescales
 341 play a more significant role during transient flow, but this significance decreases markedly
 342 for the core-scale experiments, possibly due to viscous dampening.

343 For the larger, core-scale experiments, a single spectral slope (attributed to the flow
 344 regime assumed in the multiphase extension of Darcy's law) is not observed under any
 345 of the experimental conditions explored in this work. This result suggests that the on-
 346 set of non-linear flow may occur at lower capillary numbers in larger samples. This as-
 347 sertion agrees with dynamic pore network modelling observations showing that the on-
 348 set of non-linear flow regimes start at lower flow rates as system size increases (Hansen
 349 et al., 2023; Pedersen & Hansen, 2023).

350 4 Conclusions

351 In this work we used continuous wavelet transformation to investigate sources of
 352 spectral power in the pressure time series of multiphase flow experiments. We showed
 353 that spectral power is dependent on frequency, sample size, and the heterogeneity present.
 354 Since pressure series spectral slopes are dependent on frequency and time, it is challeng-
 355 ing to extrapolate flow dynamics to larger spatial scales and longer temporal scales in
 356 a straightforward way. However, we can relate spectral signals to dynamics in the pore
 357 space. This shows how pressure time series can provide useful information about the un-
 358 derlying pore-scale dynamics at larger scales. Thus, an analysis of the pressure fluctu-
 359 ations is an important step to understanding larger scale flow processes. We showed it
 360 is possible to gain new insights into the underlying flow regimes without recourse to novel
 361 experimental techniques, or increased imaging capabilities.

362 Further work is needed to fully characterize the impact of heterogeneity, e.g. lay-
 363 ering or different lithologies, on spectral power and associated scaling regimes. Exper-
 364 iments should be conducted at lower flow rates, and different fractional flows to ascer-
 365 tain if the connected pathway flow signal observed for the pore-scale results is possible
 366 in core-scale experiments. Further work is also needed to create analytical spectra from
 367 physical models, to increase the applicability of the findings made in this work to other
 368 flow regimes and different samples.

369 5 Open Research

370 The pressure data shown in this work is attached in the Supporting Information.

371 The continuous wavelet transformation analysis is available on Github: [https://](https://github.com/Malley1/Wavelets-pycwt-wrapper)
 372 github.com/Malley1/Wavelets-pycwt-wrapper.

373 References

- 374 Akin, S., & Kovscek, A. (2003). Computed tomography in petroleum engineering re-
 375 search. *Geological Society, London, Special Publications*, 215(1), 23–38.
- 376 Avraam, D., & Payatakes, A. (1995). Flow regimes and relative permeabilities dur-
 377 ing steady-state two-phase flow in porous media. *Journal of Fluid Mechanics*,
 378 293, 207–236.
- 379 Bachu, S., & Adams, J. (2003). Sequestration of co2 in geological media in response
 380 to climate change: capacity of deep saline aquifers to sequester co2 in solution.
 381 *Energy Conversion and management*, 44(20), 3151–3175.

- 382 Benson, S. M., Bennaceur, K., Cook, P., Davison, J., de Coninck, H., Farhat, K., ...
 383 others (2012). Carbon capture and storage. *Global energy assessment-Toward*
 384 *a sustainable future*, 993.
- 385 Berg, S., Ott, H., Klapp, S. A., Schwing, A., Neiteler, R., Brussee, N., ... others
 386 (2013). Real-time 3d imaging of haines jumps in porous media flow. *Proceed-*
 387 *ings of the National Academy of Sciences*, 110(10), 3755–3759.
- 388 Blunt, M. J. (2017). *Multiphase flow in permeable media: A pore-scale perspective*.
 389 Cambridge University Press.
- 390 Boon, M., & Hajibeygi, H. (2022). Experimental characterization of h₂/water
 391 multiphase flow in heterogeneous sandstone rock at the core scale relevant for
 392 underground hydrogen storage (uhs). *Scientific Reports*, 12(1), 14604.
- 393 Daley, T. M., Ajo-Franklin, J. B., & Doughty, C. (2011). Constraining the reservoir
 394 model of an injected co₂ plume with crosswell cassm at the frio-ii brine pilot.
 395 *International Journal of Greenhouse Gas Control*, 5(4), 1022–1030.
- 396 Dance, T., LaForce, T., Glubokovskikh, S., Ennis-King, J., & Pevzner, R. (2019).
 397 Illuminating the geology: Post-injection reservoir characterisation of the co₂crc
 398 otway site. *International Journal of Greenhouse Gas Control*, 86, 146–157.
- 399 Fernandes, V., Roberts, G., White, N., & Whittaker, A. (2022). North american
 400 landscape evolution: Insights from stratigraphy, thermochronology and geo-
 401 morphology. *Authorea Preprints*.
- 402 Gao, Y., Lin, Q., Bijeljic, B., & Blunt, M. J. (2020). Pore-scale dynamics and the
 403 multiphase darcy law. *Physical Review Fluids*, 5(1), 013801.
- 404 Hansen, A., Flekkøy, E. G., Sinha, S., & Slotte, P. A. (2023). A statistical me-
 405 chanics framework for immiscible and incompressible two-phase flow in porous
 406 media. *Advances in Water Resources*, 171, 104336.
- 407 Hosseini, S. A., Lashgari, H., Choi, J. W., Nicot, J.-P., Lu, J., & Hovorka, S. D.
 408 (2013). Static and dynamic reservoir modeling for geological co₂ sequestra-
 409 tion at cranfield, mississippi, usa. *International Journal of Greenhouse Gas*
 410 *Control*, 18, 449–462.
- 411 Jackson, S. J., Agada, S., Reynolds, C. A., & Krevor, S. (2018). Characterizing
 412 drainage multiphase flow in heterogeneous sandstones. *Water Resources Re-*
 413 *search*, 54(4), 3139–3161.
- 414 Jackson, S. J., & Krevor, S. (2020). Small-scale capillary heterogeneity linked to
 415 rapid plume migration during co₂ storage. *Geophysical Research Letters*,
 416 47(18), e2020GL088616.
- 417 Juanes, R., MacMinn, C. W., & Szulczewski, M. L. (2010). The footprint of the co
 418 2 plume during carbon dioxide storage in saline aquifers: storage efficiency for
 419 capillary trapping at the basin scale. *Transport in porous media*, 82(1), 19–30.
- 420 Krevor, S. C., Pini, R., Zuo, L., & Benson, S. M. (2012). Relative permeability and
 421 trapping of co₂ and water in sandstone rocks at reservoir conditions. *Water re-*
 422 *sources research*, 48(2).
- 423 Lenormand, R., Zarcone, C., & Sarr, A. (1983). Mechanisms of the displacement of
 424 one fluid by another in a network of capillary ducts. *Journal of Fluid Mechan-*
 425 *ics*, 135, 337–353.
- 426 Li, B., & Benson, S. M. (2015). Influence of small-scale heterogeneity on upward
 427 co₂ plume migration in storage aquifers. *Advances in water resources*, 83, 389–
 428 404.
- 429 Liu, Y., San Liang, X., & Weisberg, R. H. (2007). Rectification of the bias in the
 430 wavelet power spectrum. *Journal of Atmospheric and Oceanic Technology*,
 431 24(12), 2093–2102.
- 432 McClure, J. E., Berg, S., & Armstrong, R. T. (2020). Capillary fluctuations in non-
 433 equilibrium systems. *arXiv preprint arXiv:2012.09139*.
- 434 Mendez-Diaz, S., Serrano-Garcia, J., Zenit, R., & Hernandez-Cordero, J. (2013).
 435 Power spectral distributions of pseudo-turbulent bubbly flows. *Physics of*
 436 *Fluids*, 25(4), 043303.

- 437 Mercado, J. M., Gomez, D. C., Van Gils, D., Sun, C., & Lohse, D. (2010). On bubble
438 clustering and energy spectra in pseudo-turbulence. *Journal of fluid me-*
439 *chanics*, *650*, 287–306.
- 440 Moebius, F., & Or, D. (2014). Pore scale dynamics underlying the motion of
441 drainage fronts in porous media. *Water Resources Research*, *50*(11), 8441–
442 8457.
- 443 Moura, M., Måløy, K. J., Flekkøy, E. G., & Toussaint, R. (2017). Verification of a
444 dynamic scaling for the pair correlation function during the slow drainage of a
445 porous medium. *Physical Review Letters*, *119*(15), 154503.
- 446 Muskat, M. (1938). The flow of homogeneous fluids through porous media. *Soil Sci-*
447 *ence*, *46*(2), 169.
- 448 Ni, H., Boon, M., Garing, C., & Benson, S. M. (2019). Predicting co2 residual
449 trapping ability based on experimental petrophysical properties for different
450 sandstone types. *International Journal of Greenhouse Gas Control*, *86*, 158–
451 176.
- 452 O'Malley, C. P. B., & Roberts, G. G. (2022). Wavelets-pycwt-wrapper v.0.1.1
453 (<https://github.com/Malley1/Wavelets-pycwt-wrapper>). *GitHub*. Re-
454 trieved from <https://github.com/Malley1/Wavelets-pycwt-wrapper> doi:
455 10.5281/zenodo.7357231
- 456 Pedersen, H., & Hansen, A. (2023). Parameterizations of immiscible two-phase flow
457 in porous media. *Frontiers in Physics*, *11*, 116.
- 458 Perrin, J.-C., Krause, M., Kuo, C.-W., Miljkovic, L., Charoba, E., & Benson, S. M.
459 (2009). Core-scale experimental study of relative permeability properties of co2
460 and brine in reservoir rocks. *Energy Procedia*, *1*(1), 3515–3522.
- 461 Pini, R., & Benson, S. M. (2013). Simultaneous determination of capillary pressure
462 and relative permeability curves from core-flooding experiments with various
463 fluid pairs. *Water Resources Research*, *49*(6), 3516–3530.
- 464 Pini, R., & Madonna, C. (2016). Moving across scales: a quantitative assessment
465 of x-ray ct to measure the porosity of rocks. *Journal of Porous Materials*, *23*,
466 325–338.
- 467 Ringrose, P., & Bentley, M. (2016). *Reservoir model design*. Springer.
- 468 Ringrose, P., Mathieson, A., Wright, I., Selama, F., Hansen, O., Bissell, R., ...
469 Midgley, J. (2013). The in salah co2 storage project: lessons learned and
470 knowledge transfer. *Energy Procedia*, *37*, 6226–6236.
- 471 Roberts, G. G., White, N., & Lodhia, B. H. (2019). The generation and scaling
472 of longitudinal river profiles. *Journal of Geophysical Research: Earth Surface*,
473 *124*(1), 137–153.
- 474 Roghair, I., Mercado, J. M., Annaland, M. V. S., Kuipers, H., Sun, C., & Lohse, D.
475 (2011). Energy spectra and bubble velocity distributions in pseudo-turbulence:
476 Numerical simulations vs. experiments. *International journal of multiphase*
477 *flow*, *37*(9), 1093–1098.
- 478 Rubin, E., & De Coninck, H. (2005). Ipcce special report on carbon dioxide capture
479 and storage. *UK: Cambridge University Press. TNO (2004): Cost Curves for*
480 *CO2 Storage, Part, 2*, 14.
- 481 Rücker, M., Berg, S., Armstrong, R., Georgiadis, A., Ott, H., Schwing, A., ... oth-
482 ers (2015). From connected pathway flow to ganglion dynamics. *Geophysical*
483 *Research Letters*, *42*(10), 3888–3894.
- 484 Rücker, M., Georgiadis, A., Armstrong, R. T., Ott, H., Brussee, N., Van der Linde,
485 H., ... Berg, S. (2021). The origin of non-thermal fluctuations in multiphase
486 flow in porous media. *Frontiers in Water*, *3*, 671399.
- 487 Rudnick, D. L., & Davis, R. E. (2003). Red noise and regime shifts. *Deep Sea Re-*
488 *search Part I: Oceanographic Research Papers*, *50*(6), 691–699.
- 489 Ruprecht, C., Pini, R., Falta, R., Benson, S., & Murdoch, L. (2014). Hysteretic trap-
490 ping and relative permeability of co2 in sandstone at reservoir conditions. *In-*
491 *ternational Journal of Greenhouse Gas Control*, *27*, 15–27.

- 492 Schlüter, S., Berg, S., Li, T., Vogel, H., & Wildenschild, D. (2017). Time scales of
493 relaxation dynamics during transient conditions in two-phase flow. *Water Re-*
494 *sources Research*, *53*(6), 4709–4724.
- 495 Spurin, C., Bultreys, T., Bijeljic, B., Blunt, M. J., & Krevor, S. (2019a). Inter-
496 mittent fluid connectivity during two-phase flow in a heterogeneous carbonate
497 rock. *Physical Review E*, *100*(4), 043103.
- 498 Spurin, C., Bultreys, T., Bijeljic, B., Blunt, M. J., & Krevor, S. (2019b). Mech-
499 anisms controlling fluid breakup and reconnection during two-phase flow in
500 porous media. *Physical Review E*, *100*(4), 043115.
- 501 Spurin, C., Bultreys, T., Rücker, M., Garfi, G., Schlepütz, C. M., Novak, V., ...
502 Krevor, S. (2020). Real-time imaging reveals distinct pore-scale dynamics
503 during transient and equilibrium subsurface multiphase flow. *Water Resources*
504 *Research*, *56*(12), e2020WR028287.
- 505 Spurin, C., Bultreys, T., Rücker, M., Garfi, G., Schlepütz, C. M., Novak, V., ...
506 Krevor, S. (2021). The development of intermittent multiphase fluid flow
507 pathways through a porous rock. *Advances in Water Resources*, *150*, 103868.
- 508 Spurin, C., Rücker, M., Moura, M., Bultreys, T., Garfi, G., Berg, S., ... Krevor, S.
509 (2022). Red noise in steady-state multiphase flow in porous media. *Water*
510 *Resources Research*, *58*(7), e2022WR031947.
- 511 Thiyagarajan, S. R., Emadi, H., Hussain, A., Patange, P., & Watson, M. (2022).
512 A comprehensive review of the mechanisms and efficiency of underground
513 hydrogen storage. *Journal of Energy Storage*, *51*, 104490.
- 514 Torrence, C., & Compo, G. P. (1998). A practical guide to wavelet analysis. *Bulletin*
515 *of the American Meteorological society*, *79*(1), 61–78.
- 516 van der Schaaf, J., Schouten, J., Johnsson, F., & Van den Bleek, C. (2002). Non-
517 intrusive determination of bubble and slug length scales in fluidized beds by
518 decomposition of the power spectral density of pressure time series. *Interna-*
519 *tional Journal of Multiphase Flow*, *28*(5), 865–880.
- 520 Zhang, Y., Bijeljic, B., Gao, Y., Lin, Q., & Blunt, M. J. (2021). Quantification
521 of nonlinear multiphase flow in porous media. *Geophysical Research Letters*,
522 *48*(5), e2020GL090477.
- 523 Zhao, B., MacMinn, C. W., & Juanes, R. (2016). Wettability control on multi-
524 phase flow in patterned microfluidics. *Proceedings of the National Academy of*
525 *Sciences*, *113*(37), 10251–10256.
- 526 Zou, S., Armstrong, R. T., Arns, J.-Y., Arns, C., & Hussain, F. (2018). Experimen-
527 tal and theoretical evidence for increased ganglion dynamics during fractional
528 flow in mixed-wet porous media. *Water Resources Research*.